Geophys. J. Int. (1990) **102**, 491–498

RESEARCH NOTE

The density and shear velocity contrast at the inner core boundary

P. Shearer and G. Masters

Institute of Geophysics and Planetary Physics, Scripps Institution of Oceanography, University of California, San Diego, La Jolla, CA 92093, USA

Accepted 1990 February 4. Received 1990 January 29; in original form 1989 September 15

SUMMARY

A systematic search of short-period GDSN seismograms from 1980 to 1984 at ranges from 20° to 90° identifies two probable *PKiKP* arrivals. *PKiKP*/*PcP* amplitude ratios for these phases are consistent with previous studies. However, more typically *PKiKP* is not observed, even when clear *PcP* arrivals are seen. We use these data to place upper bounds on *PKiKP*/*PcP* amplitude ratios for 100 event–station pairs. These bounds indicate that most measurements of *PKiKP* amplitudes are biased toward large values and predict reflection coefficients at the inner core boundary (ICB) which are too high. Our upper limits on *PKiKP* amplitudes roughly constrain the density jump at the ICB to be less than 1.0 g cm^{-3} and the shear velocity at the top of the inner core to be greater than 2.5 km s^{-1}, assuming a sharp discontinuity at the ICB. Upper bounds on *PKiKP*/*P* amplitude ratios at ranges between 70° and 90° are consistent with these results but are less reliable due to take-off angle differences between *P* and *PKiKP*.

Approximately 50 observed free oscillations of the Earth are sensitive to the structure of the inner core. Modern models derived from these and other mode data typically have a density jump at the ICB of 0.5–0.6 g cm^{-3}. An experiment in which we varied the mean density of the inner core indicates that the mode frequencies are roughly linear functionals of this parameter. The fit to the data is seriously degraded if the density jump is significantly different from 0.55 g cm^{-3}. Many of the modes are also strongly sensitive to the shear velocity in the inner core, and forward modelling indicates that the average inner-core shear velocity is probably 3.45 ± 0.1 km s^{-1}.

These results are compatible with the short-period *PKiKP* amplitude bounds, indicating that there is no inconsistency between *PKiKP* and normal mode data regarding the density and shear velocity structure at the inner core boundary.

Key words: body waves, free oscillations, inner core.

INTRODUCTION

While the the spherically averaged *P*-wave velocity structure of the inner core is constrained tightly by body wave data (e.g., Johnson & Lee 1985; Stark *et al.* 1986), the density and shear wave structure of the inner core are known relatively poorly. The average density of the inner core can be obtained from normal mode data, but resolution at the inner core boundary (ICB) is limited. While the free-oscillation data are consistent with a density jump of 0.5–0.6 g cm^{-3} at the ICB, studies of *PKiKP* amplitudes have indicated that the density jump may be as high as 1.6 g cm^{-3} (e.g., Bolt & Qamar 1970; Souriau & Souriau 1989). Reliable observations of *S* body waves in the inner core (e.g. *PKJKP*) have not been made, so there are no direct traveltime measurements of inner core shear velocity. Amplitude and waveform modelling of *PKP* and *PKiKP* phases have suggested models with shear wave velocities at the top of the inner core of 0 km s^{-1} [tentative hypothesis of Choy & Cormier (1983)], 2.5–3.0 km s^{-1} (Häge 1983), and 3 ± 1 km s^{-1} (Cummins & Johnson 1988a). Normal mode data constrain the average shear wave velocity of the inner core to somewhat higher values (~3.45 km s^{-1}), suggesting the possible presence of an *S*-wave velocity gradient near the surface of the inner core. The ICB could be a transition zone rather than a simple discontinuity, although the frequency content of short-period *PKiKP* waves appears to constrain such a transition zone to be less than 5 km thick (Cummins & Johnson 1988b).

Seismic constraints on inner core parameters have

important implications for physical models of the inner core. For example, the density contrast at the inner core boundary is directly related to the amount of gravitational energy that is released during any growth of the inner core (Gubbins 1977; Loper 1978; Gubbins, Masters & Jacobs 1979). Since outer core density structure is quite well constrained by the mode data and by the physical requirement that departures from adiabaticity and homogeneity be small, the density contrast at the ICB implicitly determines the density in the inner core which can be compared to values obtained from laboratory measurements of iron at high pressure (e.g., Anderson 1986; Jephcoat & Olson 1987). Similarly, measurements of the sharpness of the ICB boundary would help constrain models which hypothesize the existence of a transition zone between the inner and outer core (e.g., Loper & Fearn 1983; Morse 1986).

PKiKP/PcP AMPLITUDE STUDIES

In principle, direct information can be obtained regarding the density jump at the inner core boundary from observations of *PKiKP*. At near normal incidence, the *PKiKP* reflection coefficient depends mainly on the density and *P*-wave velocity contrast at the ICB. Since the *P* velocity jump at the ICB is known from *PKP* studies, the density contrast at the ICB can be calculated from measurements of *PKiKP* amplitudes. While in principle this calculation is straightforward, in practice it is difficult because *PKiKP* is a relatively weak phase which is rarely observed.

The calculation was first done by Bolt & Qamar (1970), who compared *PcP* and *PKiKP* amplitudes as measured at the LASA array by Engdahl, Flinn & Romney (1970). It is advantageous to compare *PKiKP* amplitudes with *PcP* amplitudes, since the phases have very similar paths in the upper mantle, and the reflection coefficient at the core–mantle boundary is relatively well known. Thus, it is only necessary to correct for differences in geometric spreading and any attenuation in the outer core in order to calculate the observed *PKiKP* reflection coefficient at the ICB. Bolt & Qamar calculated that a density jump at the ICB of about 1.6 g cm^{-3} would explain the observed *PKiKP* amplitudes. This density jump is much larger than the 0.5–0.6 g cm^{-3} found from inversions of normal mode frequency data. Subsequent *PKiKP/PcP* studies have tended to confirm this—the reported *PKiKP* amplitudes are generally higher than would be expected for ICB density contrasts of 0.6 g cm^{-3} [such as in the PREM model of Dziewonski & Anderson (1981)].

Figure 1 plots the *PKiKP/PcP* observations which have been made to date and contains LASA array data from Engdahl *et al.* (1970), Engdahl, Flinn & Massé (1974), single-station data from Buchbinder, Wright & Poupinet (1973), and Warramunga array data from Souriau & Souriau (1989). In addition, we show two single-station observations from *PKiKP* phases which we were able to identify in GDSN data (see below). The theoretical amplitude ratio from PREM ($\Delta\rho = 0.6$ g cm^{-3}) is shown, compared to that predicted for a higher ICB density contrast ($\Delta\rho =$ 1.8 g cm^{-3}). The data exhibit considerable scatter, but

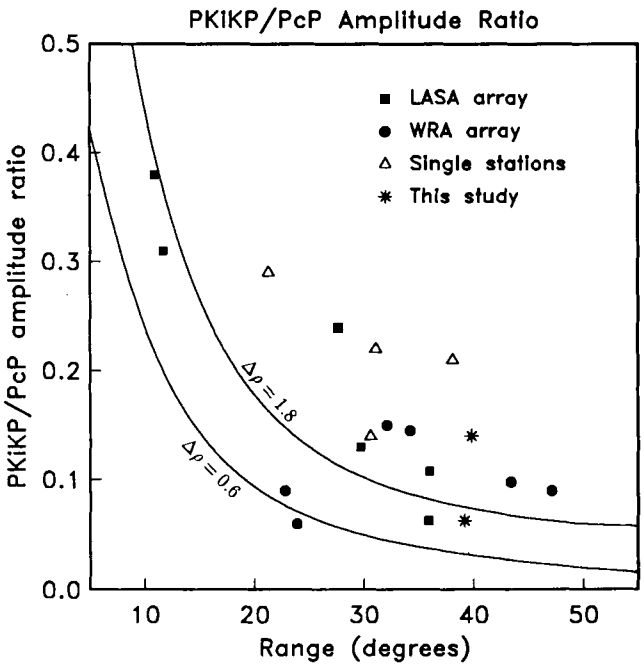

Figure 1. Observed *PKiKP/PcP* amplitude ratios plotted as a function of range. Solid squares indicate LASA array data (Engdahl *et al.* 1970, 1974); solid circles are Warramunga array data (Souriau & Souriau 1989); open triangles are single-station data from Buchbinder *et al.* (1973). The stars indicate the amplitude ratios for two *PKiKP* arrivals which we have identified in GDSN data. The lower curve shows the theoretical amplitude ratio for PREM (inner core density contrast $\Delta\alpha = 0.6$ g cm^{-3}), while the upper curve shows the result for a higher density contrast ($\Delta\rho = 1.8$ g cm^{-3}).

clearly favour models with higher ICB density contrasts than PREM.

Buchbinder *et al.* (1973) argued that *PKiKP/PcP* observations should not be used to infer the density contrast at the ICB, because individual *PcP* observations exhibit large scatter which will contaminate *PKiKP/PcP* amplitude ratios. Large scatter has been observed in *PcP* amplitudes with variations in amplitudes of 3–10 (Buchbinder & Poupinet 1973; Frasier & Chowdhury 1974). These variations could explain much of the scatter which is seen in Fig. 1. However, one should still expect that, on average, the observed *PKiKP/PcP* amplitude ratios will scatter about the 'true' amplitude ratio. For the PREM density contrast to be correct, the observed *PcP* amplitudes would need to be systematically too small, rather than simply exhibiting large scatter. However, if *PcP* amplitudes are biased it appears more likely that they are biased toward large values (Vinnik & Dashlov 1970). A more serious problem is the potential for bias in the *PKiKP* amplitude measurements. Since *PKiKP* is rarely observed above the noise, it is possible that its amplitude is only measured when it is anomalously large. Souriau & Souriau (1989) recognized this difficulty and cautioned that their *PKiKP/PcP* amplitude ratios may be larger than the true average value.

SEARCHING FOR *PKiKP*

We have systematically searched through short-period GDSN data between 20° and 90° from 1980 to 1984 looking

for *PKiKP* arrivals. There are over 4900 GDSN vertical component seismograms at these ranges within this time period which were recorded during predicted arrival times of *PKiKP*. However, for most of these records, high noise levels prevent any chance of observing *PKiKP*. We scanned through the data (available on CD-ROM for these years) with a computer algorithm which saved only those events with favourable noise levels near the predicted arrival time of *PKiKP*. In this way we reduced the number of seismograms to about 900, which we then examined interactively on a graphics terminal. We applied a 0.7–5 Hz band pass filter in order to enhance *PKiKP* relative to lower frequency signals from the coda of mantle phases (Souriau & Souriau 1989). We were able to positively identify *PKiKP* on only two records, both recorded at station CHTO (Chaing Mai, Thailand) at a range of about 40°. These events occurred on 1980 May 23 (10:32 UT) and 1980 June 16 (20:48 UT), and are both located in the Ceram Trough (east of New Guinea).

These seismograms are shown in Figs 2 and 3. The top trace is unfiltered and shows several minutes of the record and the predicted arrival times for phases *PP*, *PcP*, *S*, *PKiKP*, and *ScS*. The middle and lower traces are filtered and show 1 min of data centred on the predicted arrival times of *PcP* and *PKiKP*. Note the difference in the amplitude scaling for these two plots. Because we calculated traveltimes using PREM but used the GDSN event origin time (which assumed the JB earth model), we have adjusted our predicted times by 3 s to account for this difference. PREM traveltimes are about 3 s smaller for these phases than JB traveltimes (Dziewonski & Anderson 1981). Although the signal-to-noise ratios are fairly low, distinct *PKiKP* arrivals can be seen at the predicted times. We computed *PKiKP*/*PcP* amplitude ratios for these seismograms by picking the largest peak-to-peak amplitude for each arrival. The resulting amplitude ratios are plotted in Fig. 1. These new points fall within the scatter of *PKiKP*/*PcP* amplitude ratios obtained from previous studies.

However, on the vast majority of the records examined, *PKiKP* could not be seen, even when a clear *PcP* arrival was present. This is illustrated in Fig. 4, which shows an example (also from station CHTO) of a distinct *PcP* arrival but only noise at the appropriate arrival time for *PKiKP*. Although *PKiKP* cannot be positively identified, it is possible to estimate its maximum size from records of this type. As a first-order approximation, we simply picked the largest peak-to-peak amplitude within 5 s of the predicted *PKiKP* arrival, and took this as an upper limit to the *PKiKP* amplitude. When *PcP* could be seen, we also measured the apparent *PcP* amplitude and thus computed an upper limit to the *PKiKP*/*PcP* amplitude ratio. For example, the data shown in Fig. 4 constrain the maximum *PKiKP*/*PcP* amplitude ratio to be less than 0.049. We obtained limits on

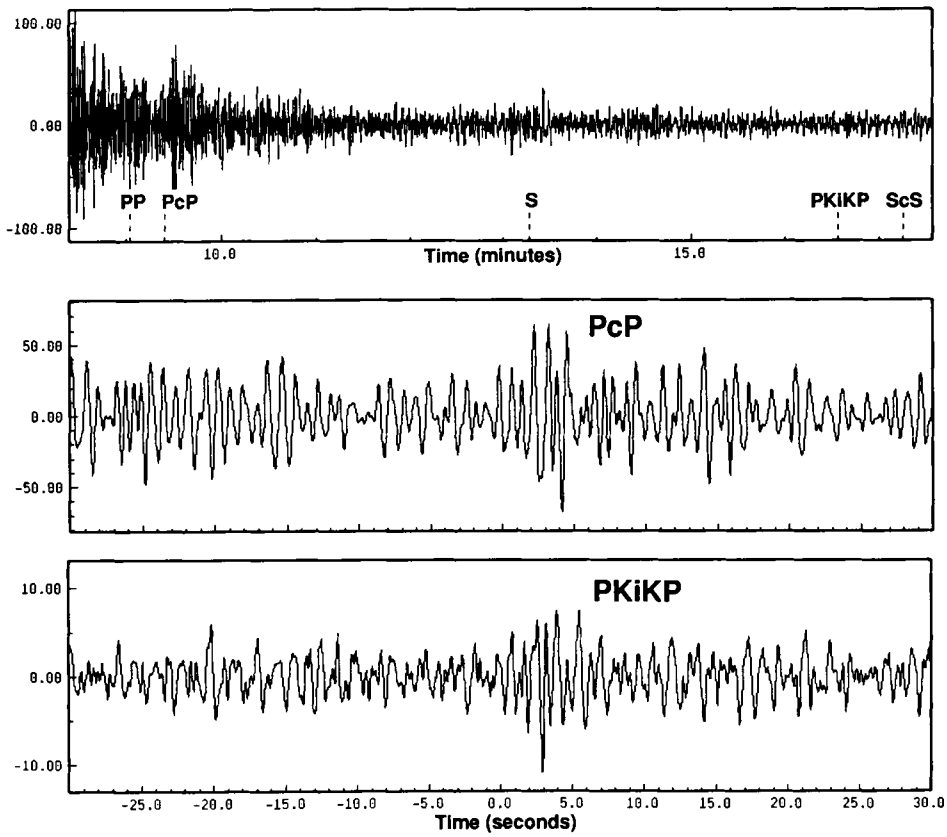

Figure 2. *PcP* and *PKiKP* arrivals for a 1980 May 23 earthquake recorded at station Chiang Mai (CHTO) in Thailand at a range of about 40°. The upper plot shows 9 min of the short-period vertical record for this event; the lower two plots show 60 s of data centred on the predicted arrival times of *PcP* and *PKiKP*—note the difference in amplitude scales for these plots. The lower traces have been band pass filtered between 0.7 and 5 Hz. The *PKiKP*/*PcP* amplitude ratio measured for this event is 0.139.

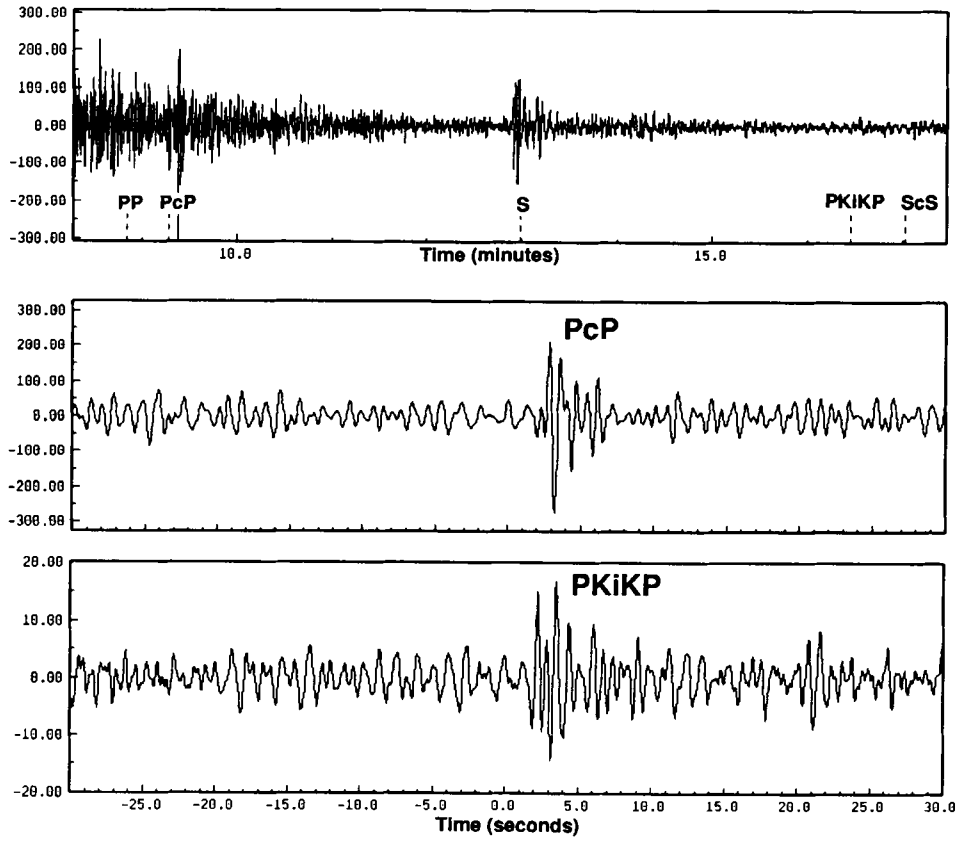

Figure 3. As Fig. 2 but for a 1980 June 16 event at a range of about 40°. The *PKiKP/PcP* amplitude ratio is 0.064.

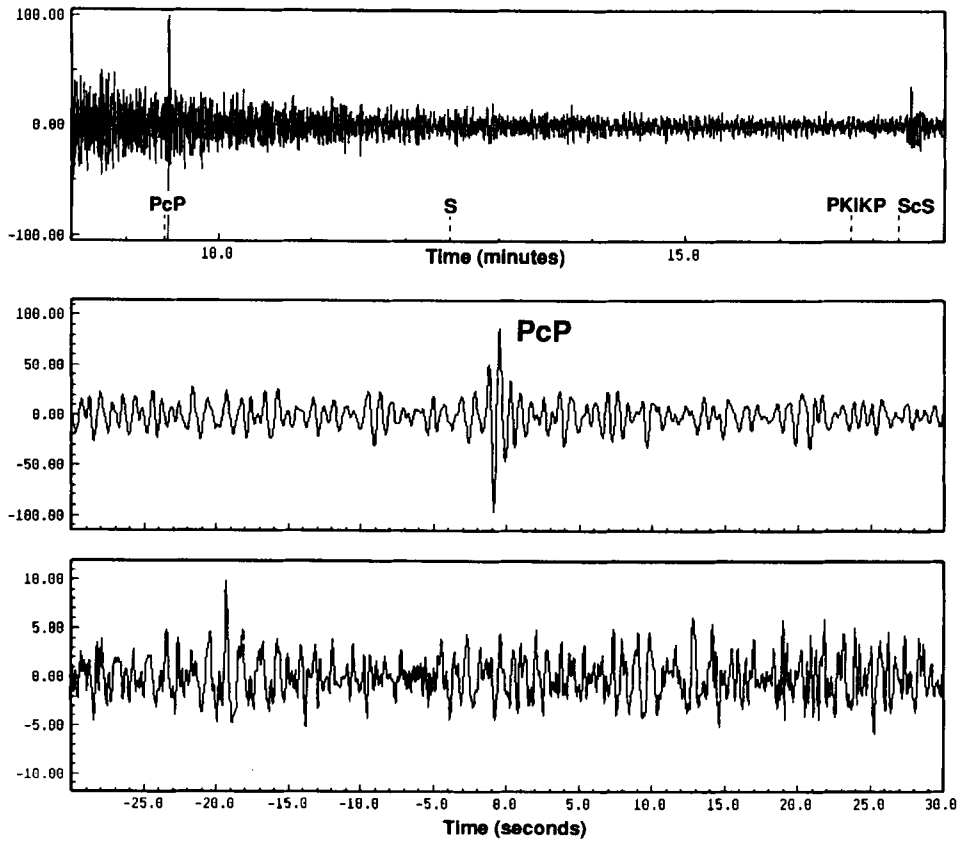

Figure 4. As Fig. 2 but for a 1980 September 14 event at a range of about 35°. *PKiKP* cannot be seen in this record. We estimate that the *PKiKP/PcP* amplitude ratio must be less than 0.049.

PKiKP/PcP from 100 records at ranges between 20° and 70°. These results are listed in Table 1 and plotted in Fig. 5. The data include records from 26 stations and 81 events.

A comparison between Fig. 1 and Fig. 5 shows that in many cases *PKiKP* should have been observed in these data if its amplitude were as high as the few actual measurements of *PKiKP* amplitudes seem to indicate. This is clear evidence that existing *PKiKP* amplitude measurements are biased towards large values. *PKiKP* is observed only when it is anomalously large, probably due to focusing from heterogeneities within the Earth. Obtaining an unbiased estimate of average *PKiKP/PcP* amplitudes is difficult since most of the data consist only of approximate upper limits. For some of the records examined, the largest peak-to-peak amplitude measured may actually have been *PKiKP*. If this arrival happened to land in a 'trough' in the noise, the computed *PKiKP* amplitude limit could be too small by up to a factor of two. However, if this were the case for many records, it is likely that other *PKiKP* arrivals would land on 'peaks' in the noise and be seen clearly. The fact that only two *PKiKP* arrivals could be identified unambiguously indicates that these amplitude limits are reasonably accurate.

Calculated *PKiKP/PcP* amplitude ratios also depend upon the measured *PcP* amplitude and could be biased toward lower values if the *PcP* amplitudes selected were anomalously high. There is some evidence for bias in *PcP* amplitudes toward large values from analysis of *PcP/P* amplitude ratios (Vinnik & Dashlov 1970). This could be a problem in our analysis at ranges below 30° and above 60° where *PcP* is seen infrequently and perhaps only when it is unusually large. However, at ranges between 30° and 60° *PcP* can be seen fairly routinely, and it is unlikely that the average *PcP* amplitudes are significantly biased within this region. Most of the scatter observed in *PcP* and *PKiKP* amplitudes is probably due to focusing effects from lateral heterogeneity in the Earth. Thus it is not surprising that the only two *PKiKP* arrivals which we identified have nearly identical ray paths for which the focusing effects should be similar.

Table 1. A list of the events and stations for which we obtained upper limits on *PKiKP/PcP* amplitudes. The columns list the earthquake year, month, day, hour, minute, depth (km), magnitude, station name, range (degrees), and measured upper limit on the amplitude ratio *PKiKP/PcP*. These upper limits are plotted as a function of range in Fig. 5.

YR	MO	DY	HR	MN	DEPTH	MAG	STA	DIST	RATIO
83	12	2	3	9	68.5	5.9	BOCO	20.0	0.2303
83	9	7	19	22	45.0	6.2	LON	20.5	0.1873
81	7	21	11	47	143.1	5.8	CTAO	20.7	0.0903
83	4	4	23	58	123.0	6.2	CTAO	20.7	0.1662
84	7	27	15	57	33.0	5.8	COL	21.0	0.2053
82	6	1	4	14	33.0	6.0	ZOBO	26.0	0.0696
82	4	17	9	20	10.3	6.2	SHIO	27.0	0.1875
82	4	19	14	42	2.1	5.8	SHIO	27.0	0.1190
80	4	13	5	41	49.0	5.9	CHTO	28.2	0.0520
82	1	25	5	29	60.0	6.1	LON	28.5	0.0518
80	7	8	4	39	178.0	5.9	CHTO	28.8	0.0450
83	1	26	16	2	238.0	6.0	TAU	29.3	0.0488
80	1	3	20	22	114.0	5.8	CHTO	29.4	0.0690
81	9	4	11	15	644.5	6.0	MAJO	29.5	0.0461
84	8	26	5	0	561.9	6.0	CTAO	30.6	0.0469
83	2	7	18	23	52.0	6.0	TAU	30.7	0.1566
82	9	17	13	28	546.0	5.9	CTAO	31.6	0.1147
84	8	26	5	0	561.9	6.0	TAU	32.5	0.1564
80	1	3	20	22	114.0	5.8	CTAO	32.6	0.1176
81	11	25	23	51	614.0	5.9	CTAO	32.6	0.0664
83	3	8	17	6	82.4	5.9	SCP	32.8	0.0579
82	7	1	7	41	47.7	6.3	MAJO	33.0	0.0553
80	7	20	21	20	591.0	6.0	CTAO	33.2	0.0639
82	1	28	16	0	0.0	5.9	COL	33.5	0.0611
84	3	1	17	45	0.0	5.9	COL	33.5	0.0537
80	9	14	2	42	0.0	6.2	ANTO	33.6	0.1351
82	1	13	0	6	33.0	6.0	TAU	33.6	0.1440
84	7	2	4	50	34.6	5.8	RSON	34.3	0.1386
82	1	25	5	29	60.0	6.1	JAS	34.4	0.0321
80	12	14	3	47	0.0	5.9	CHTO	35.0	0.0741
80	7	9	2	35	20.0	5.8	BCAO	35.0	0.1073
80	12	14	3	47	0.0	5.9	CHTO	35.0	0.0776
81	4	22	1	17	0.0	5.9	CHTO	35.0	0.1330
80	9	14	2	42	0.0	6.2	CHTO	35.1	0.0502
84	7	27	15	57	33.0	5.8	LON	35.8	0.0734
80	4	13	5	41	49.0	5.9	SHIO	36.6	0.0900
82	7	1	7	41	47.7	6.3	LON	37.3	0.0819
84	4	26	10	11	10.0	6.0	CHTO	37.3	0.1395
81	3	26	21	30	61.0	6.1	NWAO	37.7	0.0621
80	1	2	20	58	63.0	6.0	SHIO	38.2	0.0436
80	1	3	20	22	114.0	5.8	SHIO	38.2	0.0540
82	3	29	21	33	187.2	6.0	MAJO	38.2	0.0585
84	4	23	21	40	415.4	6.0	COL	38.2	0.0622
80	2	29	11	13	104.0	6.1	SHIO	38.6	0.0300
83	1	8	11	21	33.0	6.1	CTAO	38.7	0.0519
80	6	16	20	48	167.0	6.0	CHTO	39.2	0.0627
80	12	15	8	12	33.0	6.1	CTAO	39.2	0.0892
80	12	19	23	32	82.0	6.2	CHTO	39.4	0.0578
80	5	23	10	32	119.0	5.8	CHTO	39.8	0.1404
80	2	3	11	58	33.0	6.2	CTAO	40.2	0.0894
81	9	7	19	6	33.0	5.8	CHTO	40.2	0.0440
82	1	24	6	8	37.2	5.6	CTAO	40.4	0.0691
80	9	14	2	42	0.0	6.2	GRFO	42.1	0.0696
80	6	16	20	48	167.0	6.0	MAJO	44.8	0.0535
80	6	11	8	10	532.0	5.8	MAJO	45.1	0.1017
80	5	14	11	26	57.0	6.1	MAJO	45.2	0.0655
81	4	5	3	17	413.0	5.8	MAJO	45.3	0.0394
83	11	16	16	13	11.0	6.3	COL	45.8	0.0256
83	11	30	17	46	10.0	6.6	SLR	45.8	0.0511
81	11	22	15	5	24.0	6.2	CTAO	46.1	0.0992
82	12	28	13	49	34.0	6.0	CTAO	46.9	0.0776
83	10	22	13	7	33.0	6.2	BDF	47.8	0.1319
80	9	26	15	20	33.0	5.9	CHTO	47.9	0.0414
81	12	12	4	52	10.0	6.1	CTAO	48.3	0.0782
82	7	4	1	20	536.0	6.3	CTAO	48.9	0.0814
84	2	17	16	32	165.0	6.1	SHIO	49.1	0.0467
81	11	8	13	41	633.0	5.8	MAJO	49.2	0.0640
82	3	11	10	32	33.0	6.1	MAJO	49.4	0.0468
81	1	2	15	39	242.0	6.1	KAAO	49.7	0.0229
84	4	20	6	31	581.1	6.0	RSNT	49.8	0.0595
82	12	17	2	43	86.9	6.1	CTAO	50.3	0.0537
82	1	7	9	29	79.8	5.7	ZOBO	50.9	0.0398
80	12	19	23	32	82.0	6.2	CTAO	51.0	0.0736
83	8	8	3	47	24.8	5.9	COL	51.2	0.1517
81	2	16	15	48	34.0	5.4	KAAO	51.4	0.0286
82	12	20	0	33	72.4	5.9	ZOBO	51.8	0.0421
82	6	4	3	1	58.9	5.8	ALQ	52.0	0.0286
84	4	23	21	40	415.4	6.0	RSNT	52.7	0.0680
80	1	19	7	2	50.0	5.8	ANMO	52.8	0.0433
81	5	2	16	4	229.0	6.3	MAJO	52.8	0.0363
83	8	17	10	55	62.6	6.6	JAS	53.2	0.0283
82	7	1	7	41	47.7	6.3	ALQ	53.6	0.0432
82	3	28	23	24	95.0	6.1	ALQ	55.7	0.0276
82	9	15	20	22	128.3	6.0	SCP	55.7	0.0192
84	7	14	1	9	0.0	6.1	GDH	55.9	0.0398
83	8	17	10	55	62.6	6.6	RSSD	57.1	0.0459
81	8	23	12	0	40.0	6.0	JAS	57.8	0.0355
83	6	9	18	46	20.8	6.2	KEV	57.9	0.0764
81	5	28	16	10	125.0	5.9	MAJO	58.1	0.0426
80	7	8	4	39	178.0	5.9	KAAO	59.1	0.0514
84	4	20	6	31	581.1	6.0	GDH	59.6	0.0464
84	10	25	6	29	0.0	5.8	CHTO	59.8	0.1274
81	10	1	12	14	0.0	5.9	LON	59.9	0.0338
84	10	25	6	29	0.0	5.8	LON	59.9	0.0490
84	6	5	4	15	36.0	5.9	JAS	61.1	0.0553
80	2	13	22	9	63.0	6.1	BCAO	62.2	0.0282
84	4	20	6	31	581.1	6.0	RSSD	66.6	0.0591
83	7	31	10	26	10.0	5.9	LON	67.0	0.0356
80	5	18	20	2	9.0	5.7	CHTO	68.7	0.0254
84	4	23	21	40	415.4	6.0	RSON	68.8	0.0657

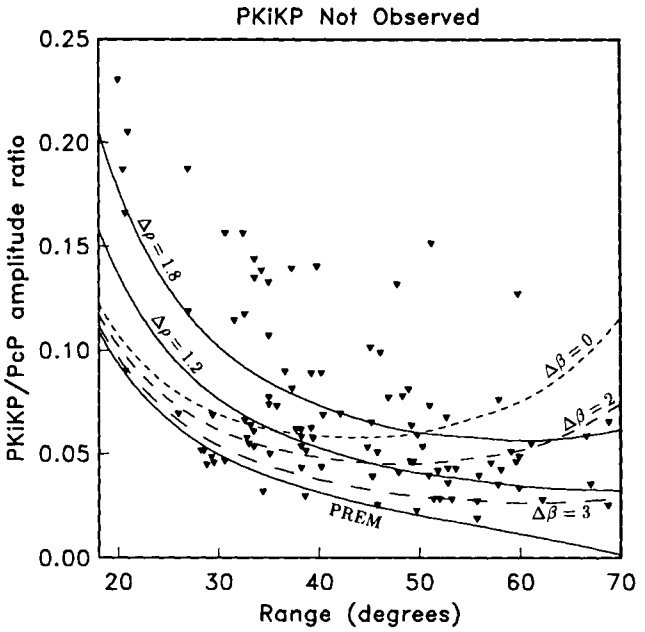

Figure 5. Upper limits on *PKiKP/PcP* amplitude ratios obtained from 100 GDSN records at ranges between 20° and 70° in which *PKiKP* could not be identified clearly. The lower solid curve shows the predicted amplitude ratio versus range for PREM (ICB density contrast $\Delta\rho = 0.6\,\mathrm{g\,cm^{-3}}$, shear velocity contrast $\Delta\beta = 3.5\,\mathrm{g\,cm^{-3}}$), while the middle and upper solid lines show the effect of increasing the density contrast to $1.2\,\mathrm{g\,cm^{-3}}$ and $1.8\,\mathrm{g\,cm^{-3}}$ respectively (keeping $\Delta\beta$ fixed). The upper, middle, and lower dashed lines show the effect of *S* velocity jumps of 0, 2, and 3 km s^{-1} respectively (keeping $\Delta\rho$ fixed).

PKiKP AMPLITUDES AND ICB PROPERTIES

The amplitude of *PKiKP* relative to *PcP* is controlled largely by the reflection coefficient at the ICB, because the reflection coefficient at the core–mantle boundary is known relatively well. Since the *P* velocity jump at the ICB is known from *PKP* studies (e.g., Johnson & Lee 1985; Stark *et al.* 1986), the reflection coefficient is effectively a function of the density and *S* velocity jump at the ICB. Fig. 5 shows theoretical *PKiKP/PcP* amplitude versus range curves for PREM (ICB $\Delta\rho = 0.6\,\mathrm{g\,cm^{-3}}$, $\Delta\beta = 3.5\,\mathrm{km\,s^{-1}}$), and additional curves which show the effect of changing these parameters. The solid curves above the PREM curve show the predicted amplitude ratios for density jumps of $1.2\,\mathrm{g\,cm^{-3}}$ and $1.8\,\mathrm{g\,cm^{-3}}$ (keeping $\Delta\beta$ fixed), while the dashed curves show the effect of S velocity jumps of 0, 2, and 3 km s^{-1} (keeping $\Delta\rho$ fixed). These calculations assume an outer core Q_α of infinity; using the actual PREM outer core Q_α of 57822 does not change these results significantly. *PKP* traveltime studies show that it is unlikely that the *P* velocity jump at the inner core boundary deviates by more than 10 per cent from the PREM value of 0.67 km s^{-1} (e.g., Häge 1983; Johnson & Lee 1985; Stark *et al.* 1986). These allowed differences are not large enough to significantly affect our conclusions concerning the more poorly known density and shear velocity contrast at the ICB.

Increasing the density jump at the ICB causes larger *PKiKP* amplitudes for all ranges shown in Fig. 5. Since the data points represent upper bounds, the density jump predicted by PREM clearly is compatible with these data. However, larger density jumps predict *PKiKP* amplitudes which are higher than our observed upper limits. We estimate that a rough upper bound on the inner core density jump is $1.0\,\mathrm{g\,cm^{-3}}$, based on our observations at ranges between 30° and 60°. Decreasing the shear velocity at the surface of the inner core has little effect on *PKiKP* amplitudes at near-normal incidence (ranges less than about 20°). At larger ranges, the effect of the *S* velocity jump becomes more important. Based on our observations between 50° and 60°, we estimate that the shear velocity at the surface of the inner core is greater than 2.5 km s^{-1}. This argues against the hypothesis of zero shear velocity at the surface of the inner core, but does allow the $\Delta\beta = 2.5$–$3.0\,\mathrm{km\,s^{-1}}$ model proposed by Häge (1983) to explain long-period *PKP* amplitude data. In deriving these limits, there is a trade-off between the density jump and the *S* velocity jump. If the density jump at the ICB were significantly less than the PREM value of $0.6\,\mathrm{g\,cm^{-3}}$, then *S* velocity jumps of less than 2.5 km s^{-1} would be permitted by these data. Similarly, if the *S* velocity jump were significantly greater than 3.5 km s^{-1}, then larger density jumps would be permitted.

Predicted *PKiKP* amplitudes for PREM drop to very small values at ranges greater than 65°. Near 72° there is a node in the *PKiKP* reflection coefficient and predicted *PKiKP* amplitudes are zero. Despite this, two *PKiKP* observations have been reported at ranges of 72° (Yellowknife Array, Buchbinder *et al.* 1973), with additional observations at ranges greater than 76° (Buchbinder *et al.* 1973; Souriau & Souriau 1989). No *PKiKP* amplitudes have been published for these observations so direct comparison with theoretical amplitudes is not possible. The amplitude of *PKiKP* at these ranges is affected strongly by the *S* velocity jump at the ICB. For example, lowering the *S* velocity jump to 3.0 km s^{-1} (from the PREM value of 3.5 km s^{-1}) removes the node in the *PKiKP* reflection coefficient and predicts much larger *PKiKP* amplitudes at ranges above 65°. The position of this node in *PKiKP* reflection coefficient depends somewhat on the *P* velocity contrast at the ICB. For example, for $\Delta\alpha = 0.60\,\mathrm{km\,s^{-1}}$ the node occurs at about 65°, while for $\Delta\alpha = 0.74\,\mathrm{km\,s^{-1}}$ the node is at about 80°.

We searched for *PKiKP* in short-period GDSN data at ranges between 70° and 90°, but did not see any clear *PKiKP* arrivals. At these ranges, *PcP* is lost in the *P* coda and cannot be used as a reference phase for *PKiKP* . As an alternative, we computed 186 maximum *PKiKP/P* amplitude ratios using the procedure described above. These points are plotted in Fig. 6. The solid curve shows the *PKiKP/P* amplitude ratio predicted by PREM, while the dashed curves show predicted ratios for *S* velocity jumps of 0, 2 and 3 km s^{-1}. The data appear to limit the shear velocity at the surface of the inner core to be greater than about 2.5 km s^{-1}, in agreement with the results obtained for *PKiKP/PcP* (See Fig. 5). However, the *PKiKP/P* amplitude ratios should be considered less reliable than the *PKiKP/PcP* ratios, due to the significant difference in ray take-off angles between *P* and *PKiKP* (16° at 80° range). Considering the very low *PKiKP* amplitudes predicted by PREM at these ranges, the fact that observations of *PKiKP* have been made (Buchbinder *et al.* 1973; Souriau & Souriau 1989), suggests that the PREM *S* velocity jump may be

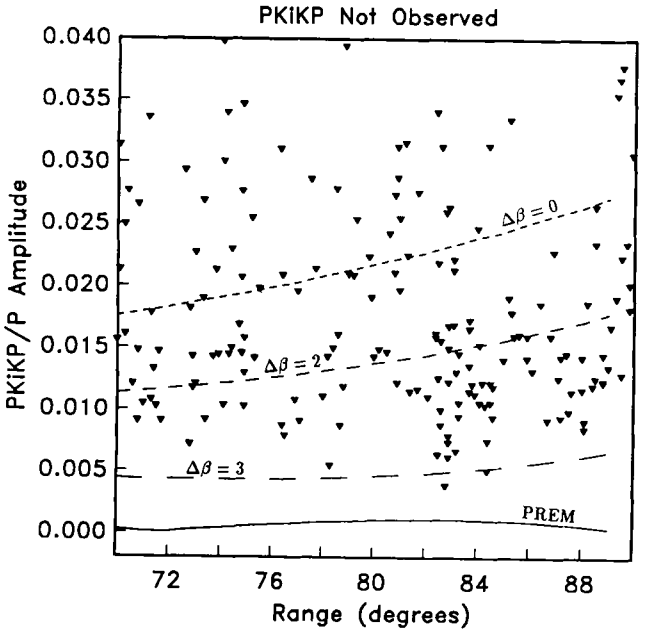

Figure 6. Upper limits on *PKiKP/PcP* amplitude ratios obtained from 186 GDSN records at ranges between 70° and 90° in which *PKiKP* could not be identified clearly. The lower solid curve shows the predicted amplitude ratio versus range for PREM (ICB density contrast $\Delta\rho = 0.6\,\mathrm{g\,cm^{-3}}$, shear velocity contrast $\Delta\beta = 3.5\,\mathrm{km\,s^{-1}}$). The upper, middle, and lower dashed lines show the effect of S velocity jumps of 0, 2, and $3\,\mathrm{km\,s^{-1}}$ respectively (keeping $\Delta\rho$ fixed).

slightly too large. Alternatively, the PREM P velocity jump ($\Delta\alpha = 0.67\,\mathrm{km\,s^{-1}}$) may be too large, since slightly smaller P velocity contrasts move the node in the *PKiKP* reflection coefficient toward closer ranges (e.g., at 65° for $\Delta\alpha = 0.60\,\mathrm{km\,s^{-1}}$), a result more consistent with the lack of any *PKiKP* observations between 50° and 70°. However, these conclusions are speculative until actual *PKiKP/P* amplitude ratios are measured at ranges above 70°.

Another factor which could influence *PKiKP* amplitudes is the possibility that the ICB is a transition zone rather than a sharp discontinuity. The thickness of such a transition zone is limited to less than 5 km by the frequency content of short-period data from LASA reflected at near-normal incidence (Cummins & Johnson 1988b). A transition zone 3 to 5 km thick would decrease short-period *PKiKP* amplitudes (relative to PREM) at ranges below 55° and increase *PKiKP* amplitudes at ranges greater than 55° (see Fig. 2 from Cummins & Johnson 1988b).

NORMAL MODE RESULTS

Inversions of an improved free-oscillation degenerate frequency data set point quite clearly to an ICB density jump of about 0.5–$0.6\,\mathrm{g\,cm^{-3}}$ (Widmer, Masters & Gilbert 1988). About 50 of the modes for which we have precise measurements are sensitive to inner core structure and starting models with different density jumps converge with few exceptions to models with $\Delta\rho \sim 0.55\,\mathrm{g\,cm^{-3}}$. While it must be noted that none of the models that have been found gives a statistically acceptable fit to this subset of the mode data (misfit is at roughly the two standard deviation level), perturbing the density jump from this value causes these modes to be much worse fit (see Fig. 7). Forward calculations also indicate that the mode frequencies are nearly linear functionals of the density in the inner core so a Backus–Gilbert resolution analysis might be meaningful. Such an analysis indicates that the free-oscillation data are unable to see details with scale lengths less than about 750 km but constrain the mean density of the inner core to a precision of better than 1 per cent. Since it is virtually certain that the density does not decrease with depth in the inner core, these results are sufficient to exclude the possibility of density jumps significantly greater than $0.55\,\mathrm{g\,cm^{-3}}$ at the inner core boundary. In particular, the density jumps of 1.2–$1.6\,\mathrm{g\,cm^{-3}}$ proposed by previous *PKiKP* amplitude studies are much too large to be compatible with the mode data.

Many of the modes are strongly sensitive to shear velocity in the inner core and models which fit the data best have a mean shear velocity of about $3.45\,\mathrm{km\,s^{-1}}$. Unfortunately, several of the modes of low harmonic degree are non-linear functionals of inner core shear velocity and change their mode characteristics dramatically with only a small change in shear velocity. This fact makes it difficult to interpret a standard resolution analysis but forward calculations indicate that the mean shear velocity in the inner core is probably $3.45 \pm 0.1\,\mathrm{km\,s^{-1}}$. As in the case with the density, details of the shear velocity structure are unresolved by the mode data so little can be said about the shear velocity immediately below the ICB. For example, a low S-wave velocity layer or gradient near the surface of the inner core boundary [such as proposed by Choy & Cormier (1983) and Häge (1983)] would not be resolvable with these data. In contrast, the *PKiKP* amplitude data discussed above are directly sensitive to the shear velocity at the surface of the inner core and appear to restrict the shear velocity contrast at the ICB boundary to $\Delta\beta > 2.5\,\mathrm{km\,s^{-1}}$.

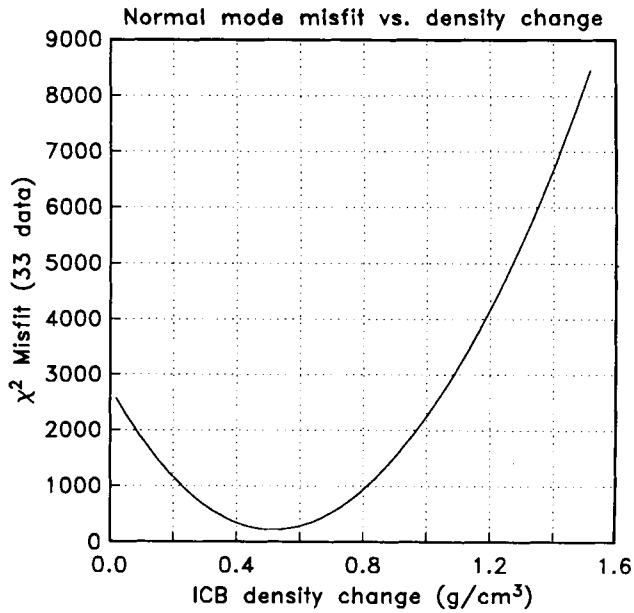

Figure 7. Misfit versus density jump at the inner core boundary for 33 normal modes sensitive to inner core density structure.

CONCLUSIONS

Upper limits on short-period *PKiKP* amplitudes can be obtained from seismograms which do not show clear *PKiKP* arrivals. These limits show that most estimates of *PKiKP* amplitudes are biased toward large values due to the difficulty of observing *PKiKP*. Upper bounds on *PKiKP/PcP* and *PKiKP/P* amplitude ratios constrain the density jump at the ICB to be less than about $1.0\,g\,cm^{-3}$ and the *S* velocity jump to be greater than $2.5\,km\,s^{-1}$, assuming a sharp discontinuity at the ICB. Normal mode analysis indicates that the average shear velocity in the inner core is $3.45 \pm 0.1\,km\,s^{-1}$ and the average inner core density is $12.9 \pm 0.13\,g\,cm^{-3}$, with a density jump at the inner core boundary of about $0.55\,g\,cm^{-3}$. These results are compatible with the short-period *PKiKP* amplitude bounds, indicating that there is no inconsistency between *PKiKP* and normal mode data regarding the density and shear velocity structure at the inner core boundary.

Finally, it is interesting to note that nutation data also constrain the density structure of the inner core (Mathews *et al.* 1990) and are dominantly sensitive to a combination of the ellipticity of the ICB and the density jump at the ICB. The value of the density jump reported here indicates that the ICB has an ellipticity which is hydrostatic with an uncertainty of about 50 per cent (P. M. Mathews, personal communication).

ACKNOWLEDGMENTS

We are grateful to A. Souriau and M. Souriau for a preprint of their paper before publication. Rudolf Widmer measured some of the modes used in our calculations. Vernon Cormier provided a helpful review of this manuscript. This study was partially supported by National Science Foundation grants EAR-87-20839 and EAR-88-16355.

REFERENCES

Anderson, O. L., 1986. Properties of iron at the earth's core conditions, *Geophys. J. R. astr. Soc.*, **84,** 561–579.

Bolt, B. A. & Qamar, A., 1970. Upper bound to the density jump at the boundary of the Earth's inner core, *Nature,* **228,** 148–150.

Buchbinder, G. G. R. & Poupinet, G., 1973. Problems related to *PcP* and the core–mantle boundary illustrated by two nuclear events, *Bull. seism. Soc. Am.*, **63,** 2047–2070.

Buchbinder, G. G. R., Wright, C. & Poupinet G., 1973. Observations of *PKiKP* at distances less than 110°, *Bull. seism. Soc. Am.*, **63,** 1699–1707.

Choy, G. L. & Cromier, V. F., 1983. The structure of the inner core inferred from short-period and broadband GDSN data, *Geophys. J. R. astr. Soc.*, **72,** 1–21.

Cummins, P. & Johnson, L. R., 1988a. Short-period body wave constraints of properties of the Earth's inner core boundary, *J. geophys. Res.*, **93,** 9058–9074.

Cummins, P. & Johnson, L., 1988b. Synthetic seismograms for an inner core transition of finite thickness, *Geophys. J.*, **94,** 21–34.

Dziewonski, A. M. & Anderson, D. L., 1981. Preliminary reference Earth model, *Phys. Earth planet. Inter.*, **25,** 297–356.

Engdahl, E. R., Flinn, E. A. & Romney, C. F., 1970. Seismic waves reflected from the Earth's inner core, *Nature,* **228,** 852–853.

Engdhal, E. R., Flinn, E. A. & Massé, R. P., 1974. Differential *PKiKP* traveltimes and the radius of the inner core, *Geophys. J. R. astr. Soc.*, **39,** 457–464.

Frasier, C. W. & Chowdhury, D. K., 1974. Effect of scattering on *PcP/P* amplitudes ratios at Lasa from 40–84° distance, *J. geophys. Res.*, **79,** 5469–5477.

Gubbins, D., 1977. Energetics of the earth's core, *J. Geophys.*, **43,** 453–464.

Gubbins, D. & Masters, T. G., 1979. Driving mechanisms for the Earth's dynamo, in *Advances in Geophysics,* pp. 1–50, Academic Press, New York.

Gubbins, D., Masters, T. G. & Jacobs, J. A., 1979. Thermal evolution of the Earth's core, *Geophys. J. R. astr. Soc.*, **59,** 57–99.

Häge, H., 1983. Velocity constraints for the inner core inferred from long-period *PKP* amplitudes, *Phys. Earth planet. Inter.*, **31,** 171–185.

Jephcoat, A. & Olson, P., 1987. Is the inner core of the Earth pure iron?, *Nature,* **325,** 322–335.

Johnson, L. R. & Lee, R. C., 1985. Extremal bounds on the *P* velocity in the earth's core, *Bull. seism. Soc. Am.*, **75,** 115–130.

Loper, D. E., 1978. The gravitationally powered dynamo, *Geophys. J. R. astr. Soc.*, **54,** 389–404.

Loper, D. E. & Fearn, D. R., 1983. A seismic model of a partially molten inner core, *J. geophys. Res.*, **88,** 1235–1242.

Mathews, P. M., Buffet, B. A., Herring, T. A. & Shapiro, I. I., 1989. The Earth's inner core: what can we learn about it from nutations?, *EOS, Trans. Am. geophys. Un.*, **70,** 301.

Morse, S. A., 1986. Adcumulus growth of the inner core, *Geophys. Res. Lett.*, **13,** 1557–1560.

Souriau, A. & Souriau, M., 1989. Ellipticity and density at the inner core boundary from sub-critical *PKiKP* and *PcP* data, *Geophys. J. Int.*, **98,** 39–54.

Stark, P. B. Parker, R. L., Masters, G., & Orcutt, J. A., 1986. Strict bounds on seismic velocity in the spherical earth. *J. geophys. Res.*, **91,** 13 892–13 902.

Vinnik, L. P. & Dashlov, G. G., 1970. PcP waves from atomic explosions and the nature of the core–mantle boundary, *Izvestiya, Phys. Solid Earth,* **1,** 7–16.

Widmer, R., Masters, G. & Gilbert, F., 1988. The spherically symmetric Earth: observational aspects and constraints on new models, *EOS, Trans. Am. geophys. Un.*, **69,** 1310.